Available online at www.sciencedirect.com

SciVerse ScienceDirect

Ceramics International 38 (2012) 4533–4540

CERAMICS INTERNATIONAL

www.elsevier.com/locate/ceramint

Photocatalytic activities of electrospun tin oxide doped titanium dioxide nanofibers

R. Nirmala [a,b], Hak Yong Kim [a,b,*], R. Navamathavan [c], Chaun Yi [d], Jeong Jin Won [a], Kyungsoo Jeon [a], Ayman Yousef [e], R. Afeesh [e], Mohamed El-Newehy [f]

[a] Department of Organic Materials and Fiber Engineering, Chonbuk National University, Jeonju 561-756, South Korea
[b] Center for Healthcare Technology & Development, Chonbuk National University, Jeonju 561 756, South Korea
[c] School of Advanced Materials Engineering, Chonbuk National University, Jeonju 561 756, South Korea
[d] Hubei Provincial Research Institute of Environmental Science, Wuhan 430072, China
[e] Bio-nano System Engineering, Chonbuk National University, Jeonju 561-756, South Korea
[f] Petrochemical Research Chair, Department of Chemistry, College of Science, King Saud University, P.O. Box: 2455 Riyadh 11451, Saudi Arabia

Received 18 January 2012; received in revised form 9 February 2012; accepted 10 February 2012
Available online 18 February 2012

Abstract

SnO_2 doped TiO_2 electropsun nanofiber photocatalysts were successfully prepared by means of electrospinning process. The surface morphology, structure and optical properties of the resultant products were characterized by field-emission electron microscopy (FE-SEM), X-ray diffraction (XRD), high-resolution transmission electron microscopy (HR-TEM), X-ray photoelectron spectroscopy (XPS), UV–vis spectroscopy, photoluminescence (PL) and cathodoluminescence (CL) techniques. The utilized physiochemical analyses indicated that the introduced SnO_2 doped TiO_2 nanofibers have a smooth surface and uniform diameters along their lengths. The photocatalytic performance of the composite nanofibers was tested for degradation of methylene blue (MB) and methyl orange (MO) dye solution under ultraviolet (UV) irradiation. Under the UV irradiation, the photocatalytic reaction rate in case of utilizing SnO_2-doped TiO_2 nanofibers was rapidly increased than that of the pristine TiO_2 nanofibers. Overall, this study demonstrates cheap, stable and effective material for photocatalytic degradation at room temperature.

Keywords: Electrospinning; Titanium dioxide; Tin oxide; Nanofibers; Photocatalyst

1. Introduction

Photocatalytic degradation of several organic contaminants using wide bandgap semiconductor nanoparticles suspended in aqueous solutions as well as immobilized semiconductor thin films has been studied extensively [1–4]. These semiconductor photocatalytic processes have shown a great potential as a low-cost, environmental friendly, and sustainable treatment technology toward the water and waste water industry. Among the numerous semiconductor photocatalyst, titanium dioxide (TiO_2) photocatalysts are of great importance due to their excellent properties such as a high photocatalytic activity, stability and nontoxicity [5–7]. TiO_2 can be utilized for the photocatalytic degradation in the form of powder, film, nanoparticles and nanotubes [8–12]. If the TiO_2 is used in the form of powder or film, post-treatment process is required to remove the suspended highly dispersed TiO_2 powder which is time consuming and increasing costs of the plant. In such case, nanotube based TiO_2 can be the appropriate materials in which larger surface area, faster electron transport and lower recombination rate resulting in a higher photocatalytic activity and efficiency [12]. One of the main goals in materials science fields is to find the proper photocatalyst with high quantum efficiency and catalytic performance. Therefore, it is important to develop the novel photocatalysts for pollutants degradation which have the proper bandgap, strong oxidative ability and high stability in water solution system.

Electrospinning technique is being used to an increasing extend to produce ultra thin nanofibers from a wide range of polymer materials [13–16]. The remarkable high surface area-to-volume ratio, small diameter and high porosity bring

* Corresponding author at: Department of Organic Materials and Fiber Engineering, Chonbuk National University, Jeonju 561-756, South Korea. Tel.: +82 63 270 2351; fax: +82 63 270 4249.
E-mail address: khy@jbnu.ac.kr (H.Y. Kim).

0272-8842/$36.00
doi:10.1016/j.ceramint.2012.02.030

electrospun nanofibers highly attractive to ultrasensitive sensors and increasing importance in many technological applications [17,18]. Recently, many research groups have already prepared TiO_2 nanofibers and it can be served as matrix modified with either the same or different materials offering another mean for increasing the surface area and enabling greater function [19–26]. However, photocatalytic activities of electrospun TiO_2 with the incorporation of SnO_2 composite nanofibers have not been investigated.

In this study, we synthesized SnO_2-doped TiO_2 nanofibers by using electrospinning technique. The obtained composite nanofibers calcined at high temperature to activate the nanofiber surfaces. The prepared composite nanofibers were analyzed by field-emission scanning electron microscopy (FE-SEM), high-resolution transmission electron microscopy (HR-TEM), energy dispersive X-ray spectrometer (EDX), X-ray diffraction (XRD), X-ray photoelectron spectroscopy (XPS). The optical properties of the resultant nanofibers were studied by using UV–visible spectrophotometer, photoluminescence (PL) and cathodoluminescence (CL) spectroscopy. The photocatalytic performance of the composite nanofibers was tested for degradation of methylene blue (MB) and methyl orange (MO) dye solution under ultraviolet (UV) irradiation. The results demonstrated that the SnO_2-doped TiO_2 composite nanofibers showed the superior photocatalytic efficiency than that of the TiO_2 nanofibers.

2. Experimental

2.1. Materials

Poly(vinyl pyrrolidone) (PVP, Mw = 1,300,000 g/mol), titanium (IV) isopropoxide (TiP, 97 assay), tin choride ($SnCl_2$, 99.5 assay) and ethanol (94.5 assay) were obtained from Samchun Co., South Korea. All these materials were used without any further purification.

2.2. Catalyst preparation

PVP solution was prepared by dissolving 0.75 g polymer into 10 ml of ethanol by means of vigorous stirring at room temperature for 3 h. The TiO_2 sol was prepared by hydrolyzing 1.5 g of TiP with a mixture of 5 ml of ethanol and 3 ml of acetic acid and then added to the prepared PVP solution for 30 min. And in the 2:3:5 ratio titanium iospropoxide:acetic acid:ethanol was added to make the sol. This sol was mixed with 10 ml PVP solution for 30 min. This colloidal solution was used to make the TiO_2/PVP nanofiber mats.

2.3. Electrospinning

The homogeneously mixed colloid was transferred into a 5 ml syringe fitted with a metallic needle of 0.4 mm of inner diameter. The syringe was fixed horizontally on the syringe pump and the positive electrode of the high voltage power supply (CPS-60K02vl, Chungpa EMT Co., South Korea), capable of generating voltages up to 60 kV, was clamped to the metal needle tip. The flow rate of polymer solution was kept at 2 μl/min, the applied voltage was 15 kV and the tip-to-collector distance was kept at 15 cm. All experiments were conducted at room temperature. The developed nanofiber mats formed were initially dried for 24 h at 50 °C under vacuum and then calcined at 550 °C in Argon ambient for 3 h, with a heating rate of 5 °C/min.

2.4. Doping of SnO_2 with TiO_2 nanofibers

For the SnO_2 doped TiO_2 composite nanofibers, $SnCl_2$ (0.2 mol/l) was dissolved in HCl solution and then the solution was gently poured in to the petri dish containing of calcined TiO_2 nanofiber mats. Careful bathing of the nanofiber mat was maintained for 12 h at room temperature and then $NH_3{\cdot}H_2O$ (5 ml) was added into the bathing for 12 h. After that the nanofiber mats were rinsed by ethanol 3 times and dried at 40 °C under vacuum condition. Finally, the dried nanofiber mats were calcined at 550 °C in air to obtain the SnO_2 doped TiO_2 composite nanofibers. The calcined mats were utilized for the further characterizations.

2.5. Characterizations

The morphology of the as-spun TiO_2/PVP and SnO_2–TiO_2 composite nanofibers was observed by using field-emission scanning electron microscopy (FE-SEM, Hitachi S-7400, Hitachi, Japan). Elemental composition analyses of the composite nanofibers were carried out using a FE-SEM equipped with an energy dispersive X-ray (EDX) spectrometer. High-resolution transmission electron microscopy (HR-TEM, JEM 2010, JEOL, Japan) images were recorded at an operating voltage of 200 kV. Structural characterization was carried out by X-ray diffraction (XRD) in a Rigaku X-ray diffractometer operated with Cu Kα radiation (λ = 1.540 Å). X-ray photoelectron spectroscopy (XPS) was carried out on an AXIS-NOVA (Kratos. Inc., Japan) with a monochromatic X-ray source of Al Ka (1486.6 eV). The base pressure during the analysis was 8.8×10^{-9} Torr. An analyzer with pass energy of 160 eV for wide scan and 20 eV for narrow scan was used. The binding energies (BE) were referenced to the adventitious C1s peak at 284.6 eV. The UV–vis spectra were measured in the range of 200–800 nm by using a UV–vis spectrometer (Lambda 900, Perkin-Elmer, USA). The optical property of the composite nanofibers was characterized by photoluminescence (PL) analysis using a 325 nm He–Cd laser and a cathodoluminescence (CL) attached to the field emission scanning electron microscopy (FE-SEM) system.

2.6. Photocatalytic activity measurements

The photocatalytic activity of the prepared composite nanofiber photocatalysts was evaluated by degradation of methylene blue and methyl orange dyes solution in a simple photochemical reactor. In the present investigation, the reactions were carried out in a cylindrical photochemical reactor which was made of glass having dimensions 10 cm × 15 cm (height × diameter), wrapped with aluminum foil. A total of 50 mg of the photocatalyst was added into 100 ml of aqueous dye

solution with an initial concentration of 10 ppm. Prior to photoreaction, the suspension was magnetically stirred in a dark condition for 30 min to establish an equilibrium status. A 40 W UV lamp (Mercury) emitting a wavelength of 295 nm was used as radiation source. The photocatalytic reaction was performed for about 100 min. At given time intervals, the approximately 2 ml samples were collected from the suspension with a pipette and immediately centrifuged to separate the residual catalyst and then the absorbance of the solution samples was measured at the corresponding wavelength via UV–vis spectrophotometer.

3. Results and discussion

Electrospinning technique has been extensively used to produce nanofibers. Fig. 1(a) and (b) shows the FE-SEM images of the as-obtained TiP/PVP and calcined TiO_2 electrospun nanofibers. As shown in these figures, the as-spun composite nanofibers with before and after calcinations were observed to be smooth surface and uniform diameters along their lengths. The diameters of these composite nanofibers were determined to be in the range of 150–200 nm. The morphology of the as-spun TiP/PVP composite nanofibers after calcination at 550 °C for 3 h in the argon is still smooth and uniform with diameter in the range of 100–150 nm, as shown in Fig. 1(b). This considerable size reduction could be attributed to the decomposition of the precursor and degradation of polymer during calcination process.

Fig. 2(a) and (b) shows the low and high-magnification FE-SEM images of the as-spun SnO_2 doped TiO_2 composite nanofibers after calcinations, respectively. Calcination of $SnCl_2$–TiO_2 composite nanofiber mats at high temperature significantly affected the general morphology of the resultant nanofibers and led to formation of SnO_2 doped TiO_2 composite nanofibers. As shown in Fig. 2, such calcination process was led to the protrusion of SnO_2 on the surfaces of the nanofibers due to the densification of the nanofiber morphology.

XRD is used to investigate the phase structures of the nanofibers obtained after calcinations from both formulations. Fig. 3 shows the obtained results. As shown in the figure, in both formulations the rutile reflections are dominating in the reflection patterns and anatase is also present. The results clearly affirmed the formation of the rutile phases, as shown in XRD data in Fig. 3. The existence of strong diffraction peaks at 2θ values of 25.25°, 35.80°, 40.50°, 42.60°, 53.9°, 55.05°, and 63.65 °corresponding to the crystal planes (1 1 0), (1 0 1), (1 1 1), (2 1 0), (2 2 1), (2 2 0), and (3 1 0), respectively, indicating the formation of the rutile (JCPDS card no 21-1272). In addition, the diffraction peaks at 24°, 47.1°, 62°, and 68.1° corresponding to the anatase phases of (1 0 1), (2 0 0), (2 0 4) and (1 1 6) planes, respectively. On the other hand, the

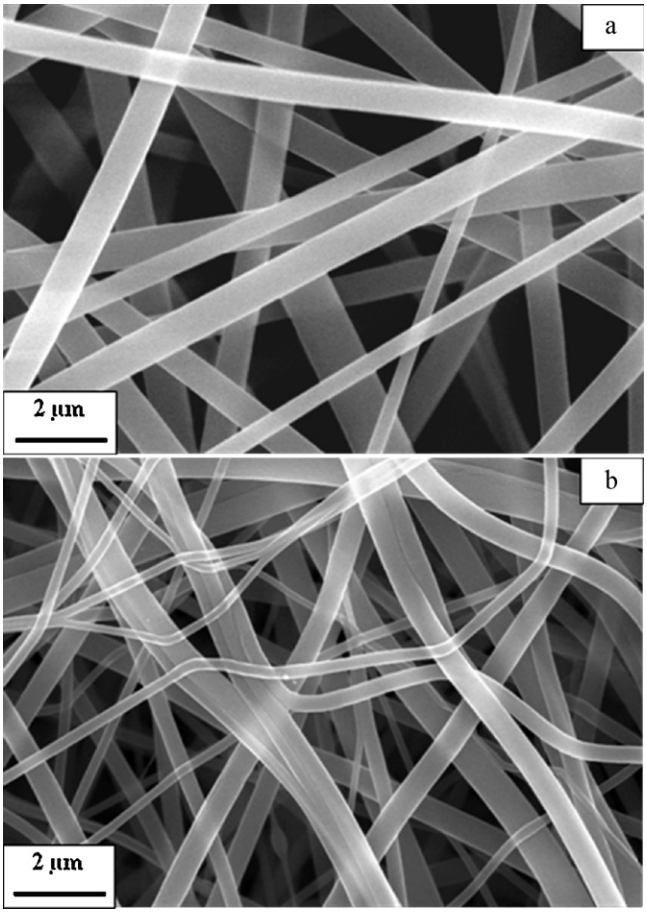

Fig. 1. FE-SEM images of TiO_2 nanofibers before (a) and after (b) calcinations.

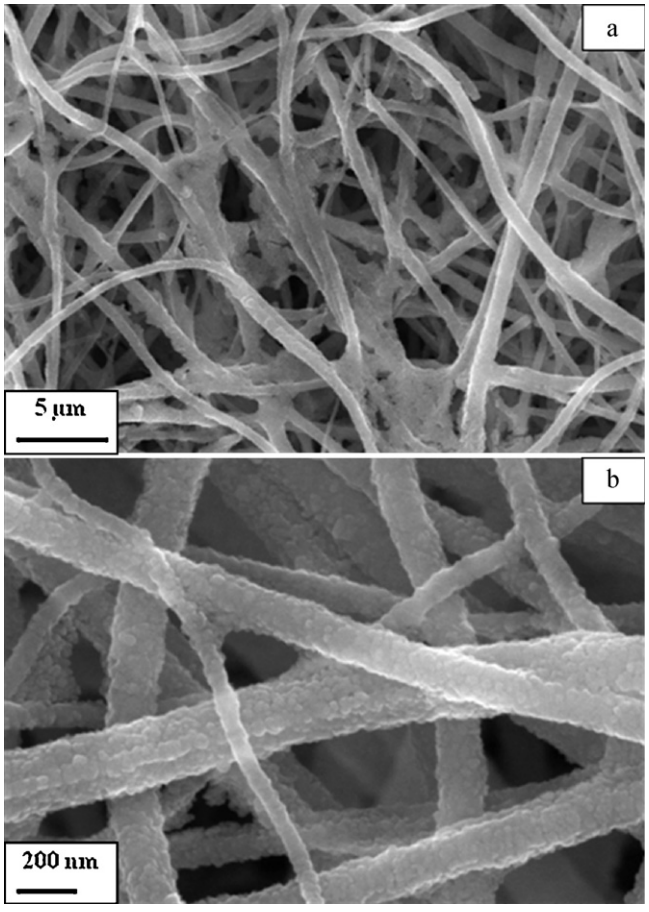

Fig. 2. FE-SEM images of SnO_2–TiO_2 composite nanofibers after calcinations (a) low and (b) high magnification.

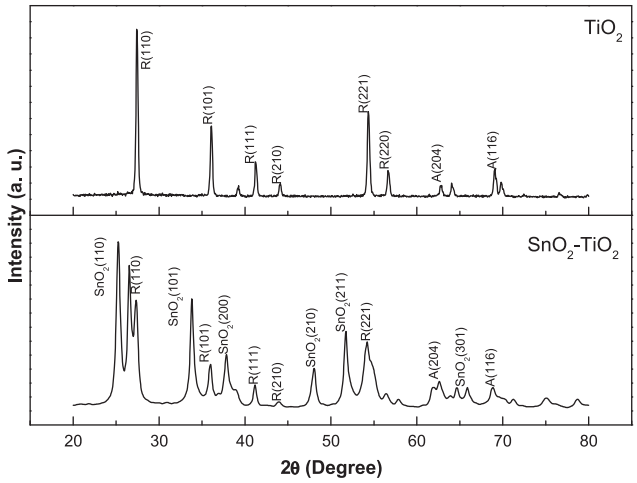

Fig. 3. XRD patterns of electrospun TiO_2 and SnO_2–TiO_2 composite nanofibers.

XRD data indicate the formation of SnO_2–TiO_2 upon calcination of $SnCl_2$–TiO_2 electrospun composite nanofibers as the dominate diffraction peaks of SnO_2 at 26.6°, 33.89°, 37.94°, 42.63°, 51.78° and 65.93° corresponding to the crystal planes of (1 1 0), (1 0 1), (2 0 0), (2 1 0), (2 1 1) and (3 0 1), respectively, are clearly observed, which is consistent with the JCPDS data (JCPDS-41-1445). No significant diffraction peaks of any other phases or impurities can be detected in the composite nanofibers, which indicate the successful blending of SnO_2 doped TiO_2 nanofiber structure.

To understand further the elemental composition of nanofibers obtained from calcination of SnO_2–TiO_2 nanofiber mat, EDX analysis was performed. As shown in Fig. 4(a), overall area was taken for the EDX analysis. The EDX spectrum clearly confirms that the SnO_2–TiO_2 composite nanofibers consist of tin, titanium and oxygen elements, as shown in Fig. 4(b). This result affirmed the blending of SnO_2 doped TiO_2 composite nanofiber which is in good agreement with that of XRD data.

In order to better understand the bonding compositions and presence of SnO_2 in the composite nanofibers, we carried out XPS analyses. Fig. 5 shows the XPS data of TiO_2 and SnO_2–TiO_2 composite nanofibers. Fig. 5(a) shows the survey scan XPS spectra of TiO_2 and SnO_2–TiO_2 composite nanofibers. The survey scan spectrum revealed that the various signatures of the electron orbital of C1s, Ti2p, O1s and Sn2d were presented in the TiO_2 composite nanofibers corresponding to the binding energies of 284, 463, 535 and 484 eV, respectively. In addition to the Ti and O peaks that are expected for TiO_2, carbon signals were observed in both samples, believed to be included during sample preparation and subsequent handling. Fig. 5(b) shows the narrow scan XPS spectrum of Ti2p electron orbital of TiO_2 and SnO_2–TiO_2 composite nanofibers. Their Ti2p XPS spectra are identical with $Ti2p_{3/2}$ and $Ti2p_{1/2}$ peaks centered at 456.1 and 461.8 eV with a binding energy difference of 5.7 eV, which are consistent with the typical values for TiO_2 [27–29]. However, the narrow scan XPS spectrum of SnO_2–TiO_2 composite nanofibers revealed a blue shift of binding energies

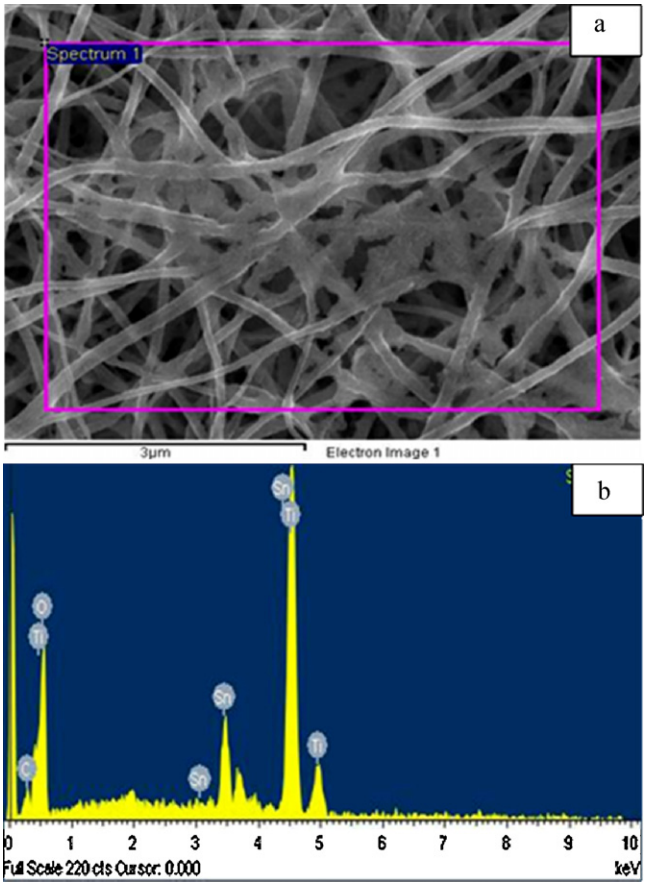

Fig. 4. (a) FE-SEM EDX spectrum of SnO_2–TiO_2 composite nanofibers, showing the presence of Sn and Ti elements in the composite nanofibers (b).

of 0.2 and 0.2 eV corresponding to $Ti2p_{3/2}$ and $Ti2p_{1/2}$ peaks centered at 456.3 and 462.0 eV, respectively. These results suggest the Sn^{2+} ions are doped in the TiO_2 lattice instead of the formation of SnO at the surface of TiO_2. When TiO_2 is doped with Sn^{2+} ions, the binding energy change in each atom occurs due to the electron transfer from Ti^{4+} to Sn^{2+}. In more detail, the Fermi level of SnO is lower than that of TiO_2. Therefore, the outer electron clouds density of Ti decreases and that of with SnO_2 incorporation. Finally, a shift in the binding energy of $Ti2p_{3/2}$ and $Ti2p_{1/2}$ were generated for the SnO_2–TiO_2 composite nanofibers as shown in Fig. 5(b). Fig. 5(c) shows the narrow scan Sn2d XPS spectra of SnO_2–TiO_2 composite nanofibers. It is clearly seen that the $Sn2d_{3/2}$ and the $Sn2d_{5/2}$ peaks exhibited corresponding to the binding energies of 492.8 and 484.1 eV, respectively. The energy difference between the two peaks is about 8.7 eV.

Fig. 6 presents the HR-TEM images of calcined SnO_2 doped TiO_2 composite nanofibers. Fig. 6(a) and (b) shows the low and high-magnification HR-TEM image of the SnO_2–TiO_2 composite nanofibers. It is clearly seen that the SnO_2 nanoparticles were spread (as shown in the arrow marks in Fig. 6(b)) in the form of well-defined and well-separated spherical particles which exhibited on the nanofiber surfaces. Fig. 6(c) shows a high-resolution HR-TEM image of the SnO_2–TiO_2 composite nanofibers. As shown in the figure, some of the SnO_2 nanoparticles were appeared to be highly crystalline nature

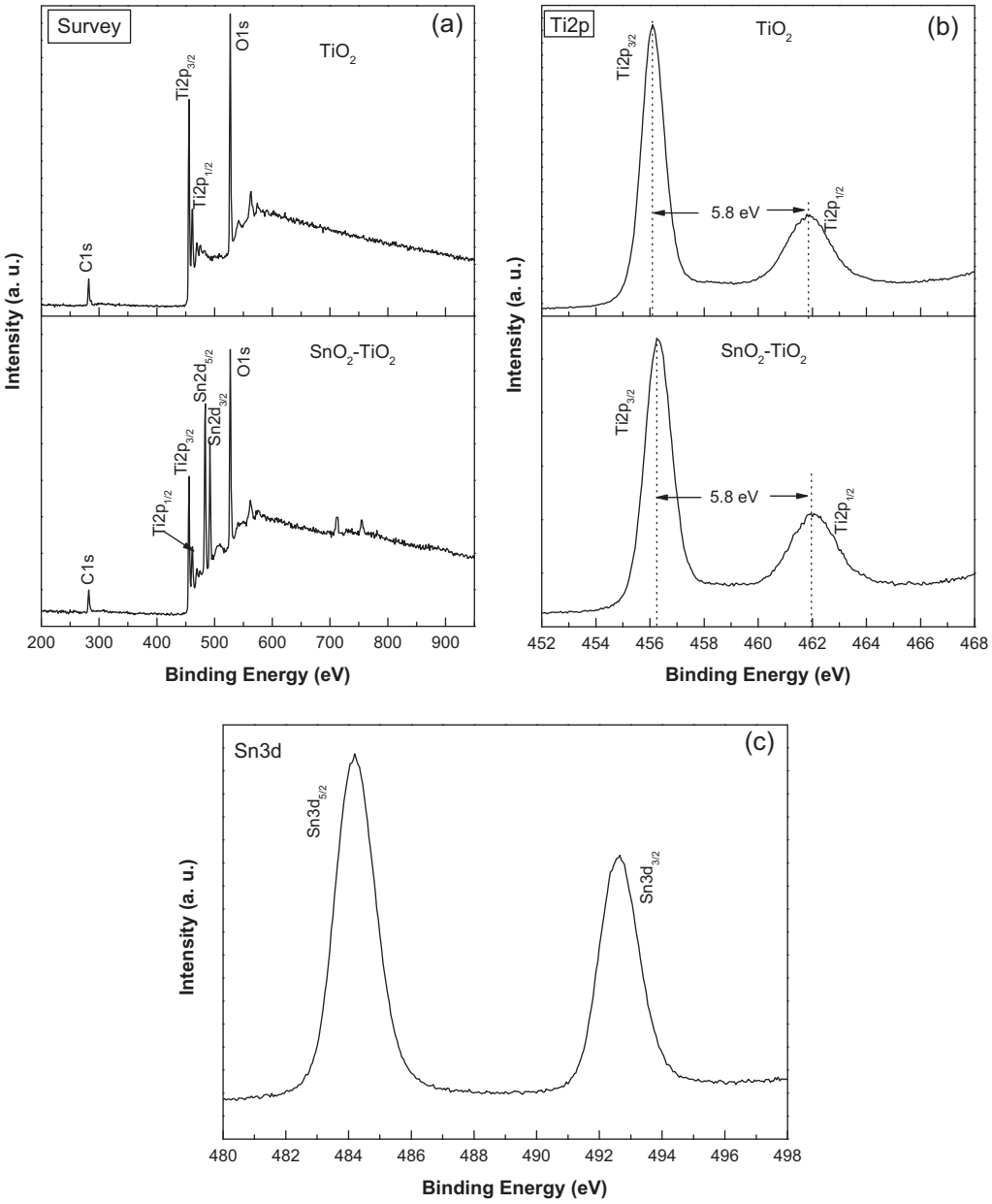

Fig. 5. XPS data of TiO_2 and SnO_2–TiO_2 composite nanofibers (a) survey spectrum, (b) narrow scan spectrum of Ti2p electron orbital; and (c) narrow scan spectrum of Sn3d electron orbital.

on the surface of the nanofiber. HR-TEM images clearly demonstrated that the SnO_2 nanoparticles were mostly attached at the periphery of nanofiber surfaces.

Fig. 7 portrays the optical absorption spectra of the TiO_2 and SnO_2 doped TiO_2 composite nanofibers. The optical spectrum of SnO_2 doped TiO_2 nanofibers displayed a red shift in the band gap transition. It was reported that similar shift was resulted from the incorporation of metal ions into the SnO_2 nanoparticles [30]. Red shift of this type could be attributed to the charge-transfer transitions between the metal ions d-electrons and the SnO_2 conduction or valence band [31].

The luminescence properties of TiO_2 and SnO_2–TiO_2 are useful in understanding the physics of nanostructures and their potential applications in various fields. Fig. 8 shows the room-temperature PL spectrum of the electrospun TiO_2 and SnO_2–TiO_2 composite nanofibers. The PL spectrum is dominated by the broad band emission in the range of 350–600 nm. A broad green photoluminescence peak in the visible range centered at about 525 nm was only detected in TiO_2 nanofibers and could be attributed to the radiative recombination of self-trapped excitons localized within the surface defects of nanofibers [32,33]. The broad band emission from the PL spectrum at room temperature indicates that the TiO_2 and SnO_2–TiO_2 composite nanofibers have good luminescence quality. According to the literature, the intensity of the PL peaks is an indicator for the electrons/hole recombination rate, low intensity indicates low recombination and vice versa. As shown in the figure, incorporation of SnO_2 leads to increase the PL intensity which preliminarily claims good photoactivity for the SnO_2-doped TiO_2 composite nanofibers compared with the pristine one.

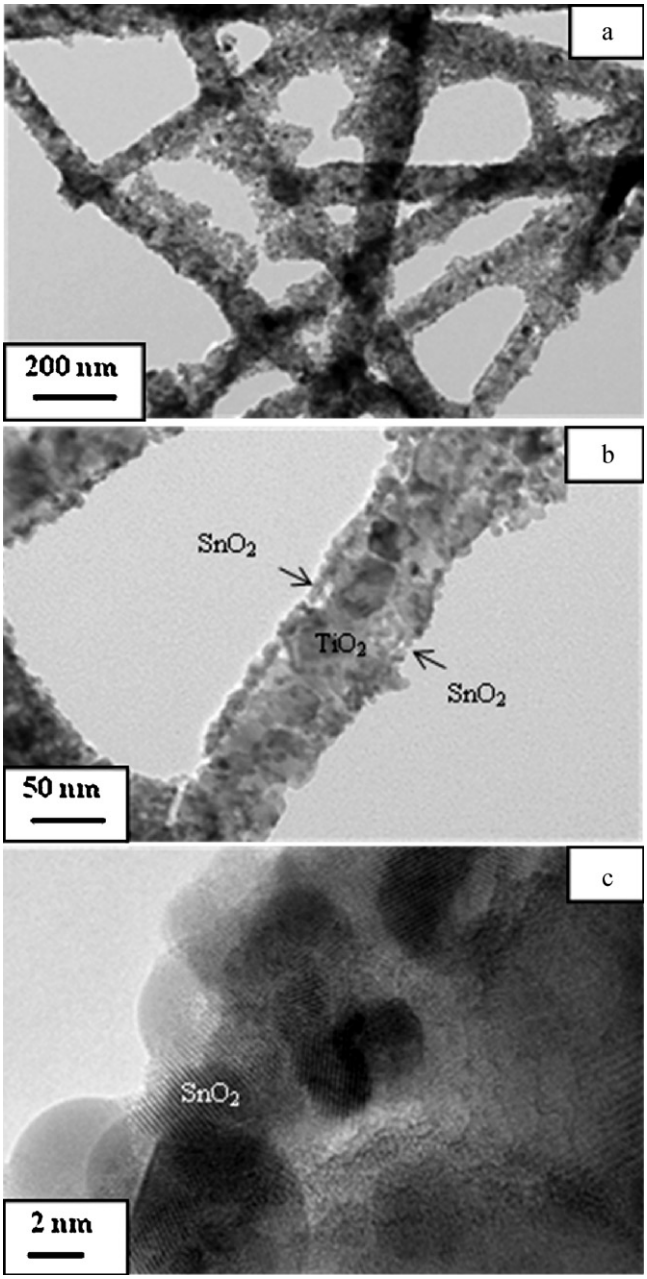

Fig. 6. HR-TEM images of SnO_2–TiO_2 composite nanofibers (a) low, (b) high resolution images, and (c) high magnification image.

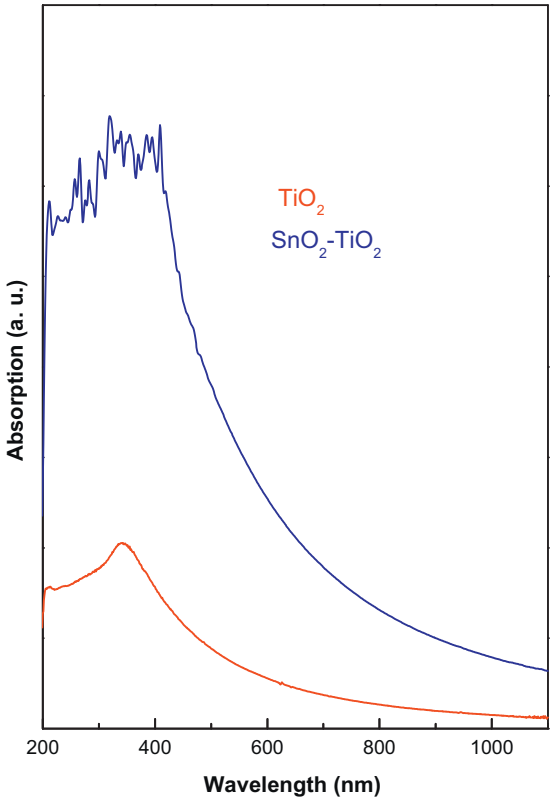

Fig. 7. UV–vis spectra of electrospun TiO_2 and SnO_2–TiO_2 composite nanofibers.

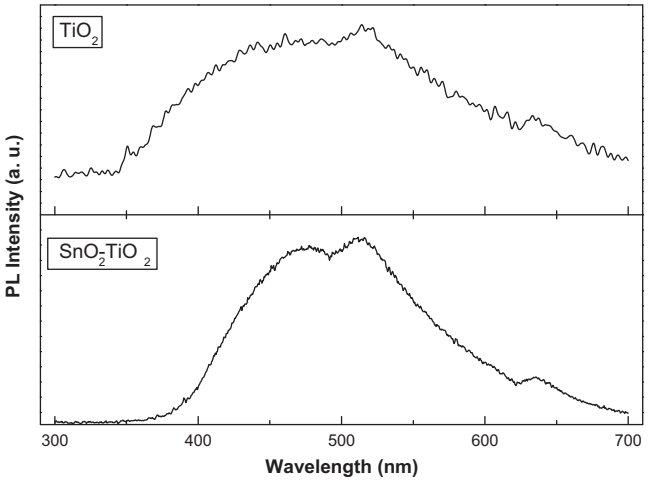

Fig. 8. PL spectra of electrospun TiO_2 and SnO_2–TiO_2 composite nanofibers.

The representative CL spectrum of electrospun TiO_2 and SnO_2–TiO_2 composite nanofibers is shown in Fig. 9, which has identical shape as the PL emission spectrum. The CL spectrum of the as-spun TiO_2 and SnO_2–TiO_2 composite nanofibers shows an overlapping of two broad emission bands due to the contribution SnO_2 and TiO_2 centered at about 475 and 550 nm, respectively.

The photocatalytic activities of the as-prepared samples were evaluated by measuring the degradation of MB and MO dyes in aqueous solutions under UV irradiation. Fig. 10(a) represents the conversion ratio of MB dye in the presence of prepared photocatalysts. MO is one of the typical azo dyes which occupy the main part of dye pollutants and often become toxic to organisms, so we selected MO to test the performance of the as-prepared catalysts. Fig. 10(b) shows the conversion ratio in MO for different photocatalysts. As shown in Fig. 10, the degradation efficiency of MO is lower than that of the MB due to the different nature of dyes. However, photocatalytic activity results of the catalysts are consistent with the MB decomposition experiment. SnO_2–TiO_2 composite nanofibers achieve the highest degradation efficiency, which is greater than that of pure TiO_2 nanofibers.

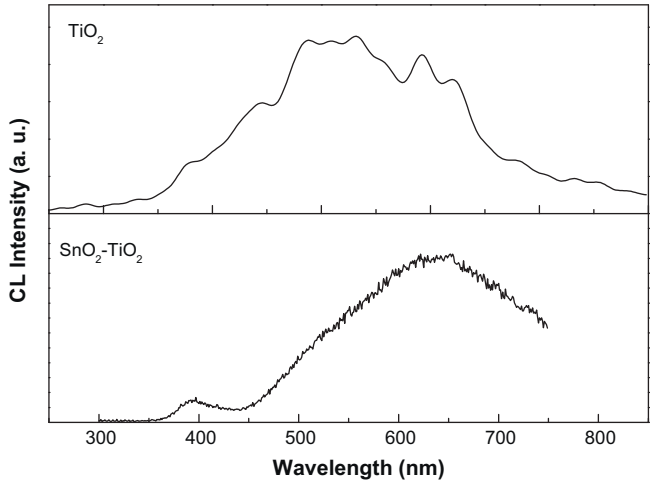

Fig. 9. CL spectra of electrospun TiO_2 and SnO_2–TiO_2 composite nanofibers.

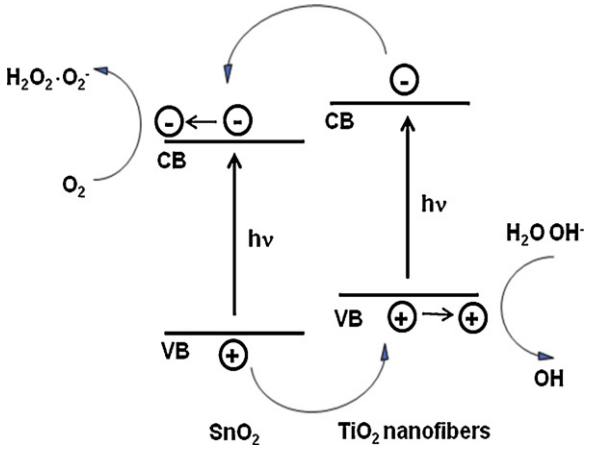

Fig. 11. Schematic diagram illustrating the charge transfer process in the SnO_2–TiO_2 composite nanofiber photocatalyst.

Based on the experimental results, SnO_2 doped TiO_2 composite nanofibers exhibited the highest photocatalytic efficiency. Two aspects may result the enhancement. For one thing, incorporated SnO_2 in TiO_2 nanofibers provides more reaction sites for the adsorption of reactants molecules, making the photocatalytic process more efficient. For another, well controlled SnO_2 particles deposited on the TiO_2 nanofibers surface can act as electron–hole separation centers. When metallic SnO_2 doped in to TiO_2 nanofibers, photogenerated electrons accumulate at metallic Sn and form a Schottky barrier at metal–semiconductor contact region, thus it promotes the photodegradation efficiency. It may be explained that SnO_2 nanoparticles cover and occupy lots of TiO_2 catalyst surface and will become new recombination centers of photogenerated electrons and holes as well, resulting in the increase of photocatalytic activity.

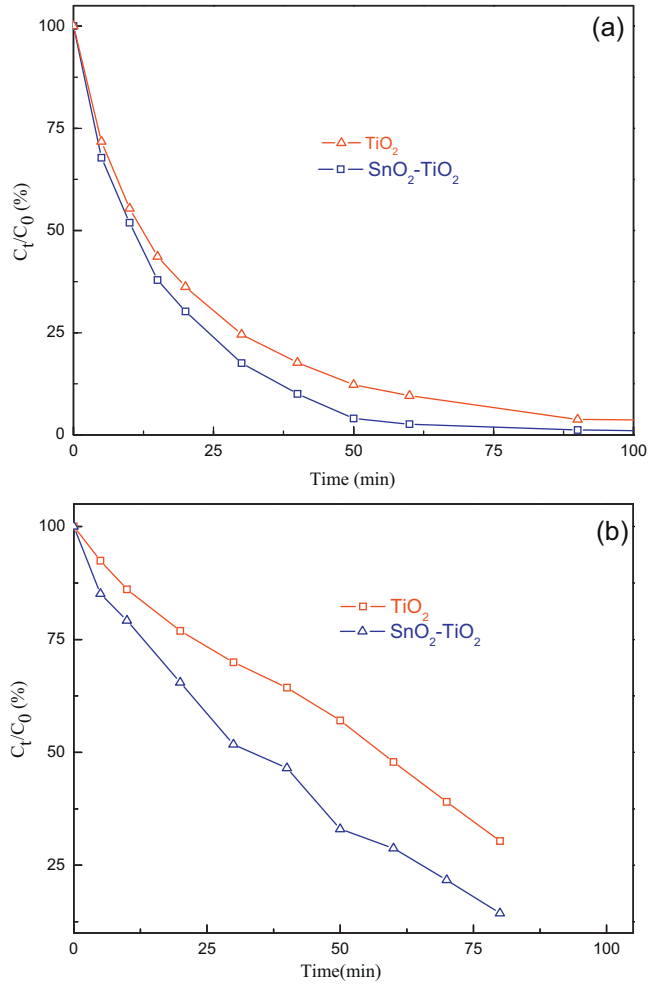

Fig. 10. Photocatalytic degradation of (a) methylene blue and (b) methyl orange by different electrospun nanofiber catalyst.

To understand further information about the degradation mechanism of MB and MO over the composite nanofibers, we proposed the schematic diagram of the charge transfer process in the SnO_2 doped TiO_2 composite nanofibers, as illustrated in Fig. 11. During the photocatalytic reaction, the absorption of a photon by TiO_2 nanofibers led to the ejection of an electron from the valence band to the conduction band of TiO_2 nanofibers and then the electron can be transferred to the conduction band of SnO_2 which is doped in to the TiO_2 nanofibers. In other words, the conduction band of SnO_2 can act as the sink for the photogenerated electrons. On the other hand, the photogenerated holes can be moved toward the opposite direction where they accumulated in the valence band of TiO_2 nanofibers resulting in an enhanced electron–hole separation.

4. Conclusions

In summary, we successfully obtained TiO_2 and SnO_2–TiO_2 composite nanofibers by using electrospinning process. These as-spun nanofibers were observed to be smooth with uniform diameters along their lengths. The photocatalytic activities of these composite nanofibers were investigated in the presence of MB and MO dyes. It was observed that the highest amount of photocatalytic efficiency was exhibited by the SnO_2 doped TiO_2 composite nanofibers The reason for better photocatalytic activity for the SnO_2 doped TiO_2 composite nanofibers as compared to TiO_2 composite nanofibers is due to the efficient electron–hole separation, which inhibits recombinations, thus

improving the photoefficiency of the SnO_2 catalyst. The photocatalytic experimental results are in good agreement with the XPS data, indicating the bonding configuration strongly influencing the photocatalytic efficiency.

Acknowledgments

This work was supported by the grant of the Korean Ministry of Education, Science and Technology (The Regional Core Research Program/Center for Healthcare Technology & Development, Chonbuk National University, Jeonju 561-756, Republic of Korea). One of the authors Hak Yong Kim kindly acknowledges King Saud University, Riyadh, Saudi Arabia for offering visiting professorship.

References

[1] K. Vinodgopal, I. Bedja, P.V. Kamat, Nanostructured semiconductor films for photocatalysis. Photoelectrochemical behavior of SnO_2/TiO_2 coupled systems and its role in photocatalytic degradation of a textile azo dye, Chem. Mater. 8 (1996) 2180–2187.

[2] H. Tada, A. Hattori, Y. Tokihisa, K. Imai, N. Tohge, S. Ito, A patterned-TiO_2/SnO_2 bilayer type photocatalyst, J. Phys. Chem. B 104 (2000) 4585–4587.

[3] M.W. Xu, S.J. Bao, X.G. Zhang, Enhanced photocatalytic activity of magnetic TiO_2 photocatalyst by silver deposition, Mater. Lett. 59 (2005) 2194–2198.

[4] J. Bandara, R.A.S.S. Ranasinghe, The effect of MgO coating on photocatalytic activity of SnO_2 for the degradation of chlorophenol and textile colorants; the correlation between the photocatalytic activity and the negative shift of flatband potential of SnO_2, Appl. Catal., A 319 (2007) 58–63.

[5] J. Yun, D. Jin, Y.S. Lee, H. Kim, Photocatalytic treatment of acidic waste water by electrospun composite nanofibers of pH-sensitive hydrogel and TiO_2, Mater. Lett. 64 (2010) 2431–2434.

[6] Z. Zhang, C. Shao, L. Zhang, X. Li, Y. Liu, Electrospun nanofibers of V-doped TiO_2 with high photocatalytic activity, J. Colloid Interface Sci. 351 (2010) 57–62.

[7] T. He, Z. Zhou, W. Xu, F. Ren, H. Ma, J. Wang, Preparation and photocatalysis of TiO_2-fluoropolymer electrospun fiber nanocomposites, Polymer 50 (2009) 3031–3036.

[8] J. Richardson, A.J. Matchett, J.M. Coulthard, S. Gibbon, C. Wilson, C. Watson, The characterization of pigment powders for titanium dioxide polymer dispersions by the 'masterbatch' process, Chem. Eng. Res. Des. 78 (2000) 39–48.

[9] G.T. Lim, K.H. Kim, J. Park, S.H. Ohk, J.H. Kim, D.L. Cho, Synthesis of carbon-doped photocatalytic TiO_2 nano-powders by AFD process, J. Ind. Eng. Chem. 16 (2010) 723–727.

[10] D. Wang, L. Xiao, Q. Luo, X. Li, J. An, Y. Duan, Highly efficient visible light TiO_2 photocatalyst prepared by sol–gel method at temperatures lower than 300 °C, J. Hazard. Mater. 192 (2011) 150–159.

[11] N. Negishi, K. Takeuchi, T. Ibusuki, The surface structure of titanium dioxide thin film photocatalyst, Appl. Surf. Sci. 121–122 (1997) 417–420.

[12] J. Liao, S. Lin, L. Zhang, N.Q. Pan, X. Cao, J. Li, Photocatalytic degradation of methyl orange using a TiO_2/Ti mesh electrode with 3D nanotube arrays, ACS Appl. Mater. Interface 4 (2012) 171–177.

[13] D. Li, Y. Xia, Electrospinning of nanofibers: reinventing the wheel? Adv. Mater. 16 (2004) 1151–1170.

[14] K. Jayaraman, M. Kotaki, Y. Zhang, X. Mo, S. Ramakrishna, Recent advance in polymer nanofibers, J. Nanosci. Nanotechnol. 4 (2004) 52–65.

[15] R. Dersh, M. Steinhart, U. Boudriot, A. Greiner, J.H. Wendorff, Nanoprocessing of polymers: applications in medicine, sensors, catalysis, photonics, Polym. Adv. Technol. 16 (2005) 276–282.

[16] Z.M. Huang, Y.Z. Zhang, M. Kotaki, S. Ramakrishna, A review on polymer nanofibers by electrospinning and their applications in nanocomposites, Compos. Sci. Technol. 63 (2003) 2223–2253.

[17] D.H. Tong, P.D. Tran, X.T.T. Pham, V.B. Pham, T.T.T. Le, M.C. Dang, C.J.M.V. Rijn, The nanofabrication of Pt nanowire arrays at the wafer-scale and its application in glucose detection, Adv. Nat. Sci.: Nanosci. Nanotechnol. 1 (2010) 015011–15014.

[18] E.P. Lee, Y. Xia, Growth and patterning of Pt nanowires on silicon substrates, Nano Res. 1 (2008) 129–137.

[19] L.S. Yoong, F.K. Chong, B.K. Dutta, Development of copper-doped TiO_2 photocatalyst for hydrogen production under visible light, Energy 34 (2009) 1652–1661.

[20] F.C. Wang, C.H. Liu, C.W. Liu, J.H. Chao, C.H. Lin, Effect of Pt loading order on photocatalytic activity of Pt/TiO_2 nanofiber in generation of H_2 from neat ethanol, J. Phys. Chem. C 113 (2009) 13832–13840.

[21] C. Wang, C. Shao, X. Zhang, Y. Liu, Inorg SnO_2 nanostructures-TiO_2 nanofibers heterostructures: controlled fabrication and high photocatalytic properties, Inorg. Chem. 48 (2009) 7261–7268.

[22] D.G. Huang, S.J. Liao, J.M. Liu, Z. Dang, L. Petrik, Preparation of visible-light responsive N–F-codoped TiO_2 photocatalyst by a sol–gel-solvothermal method, J. Photochem. Photobiol. A 184 (2006) 282–288.

[23] S. Chuangchote, J. Jitputti, T. Sagawa, S. Yoshikawa, Photocatalytic activity for hydrogen evolution of electrospun TiO_2 nanofibers, ACS Appl. Mater. Interface 1 (2009) 1140–1143.

[24] T. Cao, Y. Li, C. Wang, C. Shao, Y. Liu, A facile in situ hydrothermal method to $SrTiO_3$/TiO_2 nanofiber heterostructures with high photocatalytic activity, Langmuir 27 (2011) 2946–2952.

[25] S.H. Hwang, C. Kim, J. Jang, SnO_2 nanoparticle embedded TiO_2 nanofibers – highly efficient photocatalyst for the degradation of rhodamine B, Catal. Commun. 12 (2011) 1037–1041.

[26] Z. Liu, D.D. Sun, P. Guo, J.O. Leckie, An efficient bicomponent TiO_2/SnO_2 nanofiber photocatalyst fabricated by electrospinning with a side-by-side dual spinneret method, Nano Lett. 7 (2007) 1081–1085.

[27] X. Chen, L. Liu, P.Y. Yu, S.S. Mao, Increasing solar absorption for photocatalysis with black hydrogenated titanium dioxide nanocrystals, Science 331 (2011) 746–750.

[28] M.S. Lazarus, T.K. Sham, X-ray photoelectron spectroscopy (XPS) studies of hydrogen reduced rutile (TiO_{2-x}) surfaces, Chem. Phys. Lett. 92 (1982) 670–673.

[29] N.C. Saha, H.G. Tomkins, Titanium nitride oxidation chemistry: an X-ray photoelectron spectroscopy study, J. Appl. Phys. 72 (1992) 3072–3079.

[30] C. Wang, D.W. Bahnemann, J.K. Dohrmann, A novel preparation of iron-doped TiO_2 nanoparticles with enhanced photocatalytic activity, Chem. Commun. 16 (2000) 1539–1540.

[31] Z.J. Li, B. Hou, Y. Xu, D. Wu, Y.H. Sun, Studies of Fe-doped SiO_2/TiO_2 composite nanoparticles prepared by sol–gel-hydrothermal method, J. Mater. Sci. 40 (2005) 3939–3943.

[32] W.F. Zhang, M.S. Zhang, Z. Yin, Q. Chen, Photoluminescence in anatase titanium dioxide nanocrystals, Appl. Phys. B: Lasers Opt. 70 (2000) 261–265.

[33] J. Liqiang, S. Xiaojun, C. Weimin, X. Zili, D. Yaoguo, F. Honggang, The preparation and characterization of nanoparticle TiO_2/Ti films and their photocatalytic activity, J. Phys. Chem. Solids 64 (2003) 615–623.